

# Thiamin Deprotonation Mechanism. Carbanion Development Stabilized by the LUMOs of Thiazolium and Pyrimidylimine Working in Tandem and Release Governed by a H-Bond Switch

Donald B. DuPré\* and John L. Wong\*

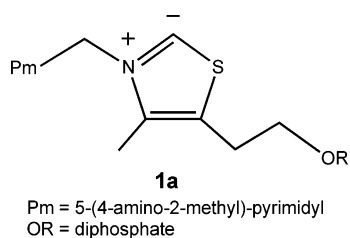
Department of Chemistry, University of Louisville, Louisville, Kentucky 40292

Received: November 6, 2006; In Final Form: January 6, 2007

Our previous paper (*J. Phys. Chem. A* 2005, 109, 7606) using computed atomic charges, based on the quantum theory of atoms in molecules (QTAIM), on azolium models of thiamin diphosphate has shown that only sulfur acts as an effective electron sink in the formation of the thiamin carbanion intermediate. Herein we apply natural bond orbital (NBO) theory to the analysis of orbital contributions to canonical molecular orbitals (CMOs) of six abbreviated azolium analogs of the carbanion to better understand the unique function of sulfur. The NBO/CMO data provide a description of the origin of the first thiamin electron sink: sulfur performing in the  $\sigma$ - and  $\pi$ -orbitals of the transition state as well as in the carbanion, and its advantages due to low electronegativity and moderate size. At the next level of thiamin modeling, we include the six-membered pyrimidine ring to represent the prerequisite V-structure in the iminopyrimidine tautomeric form. This model is subjected to incremental deprotonation and MO decomposition. The 4'-pyrimidylimine moiety, in addition to being an internal base to abstract the C2 proton, also performs as the second electron sink. Thus, the LUMOs of the thiazolium and pyrimidylimine systems working in tandem stabilize the developing charges in these transient structures, with facilitation from their HOMOs. Further, the absence of detectable amounts of the C2 carbanion in  $^{13}\text{C}$ -labeled thiamin–enzyme complex by NMR is explained. Both NBO analysis and the QTAIM topological electronic properties suggest the operation of a H-bonding scheme that leads to the formation of a cryptic C2 carbanion that is not accumulated. The shielding of the carbanion by the N4'–H hydrogen bond is weakened by N1'–H deprotonation. Consequently, prior return of the N1' proton to the nearby glutamate may be the switch for streaming a timed-release of the unstable C2 carbanion to the incoming substrate.

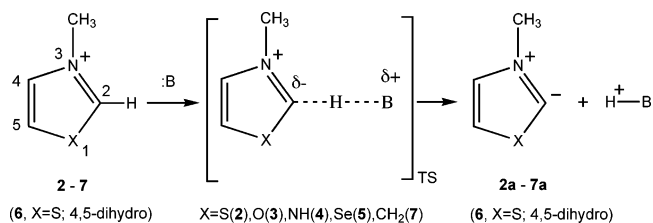
## Introduction

A broad range of reactions catalyzed by decarboxylase and transketolase require thiamin diphosphate (ThDP) as a carbon acid to generate an acyl carbanion synthon, **1a**.<sup>1–4</sup> The carbanion



is assumed to be stabilized by electron delocalization into the thiazolium ring. We have previously investigated the mechanism of stabilization of this unusual carbanion by applying the quantum theory of atoms in molecules<sup>5,6</sup> (QTAIM) to acquire charge distributions in thiazolium **2** and the X-substituted analogs oxazolium **3**, and imidazolium **4**.<sup>7</sup> In these abbreviated models (see Scheme 1), which are focused on the electronic properties of the five-membered ring, the aminopyrimidine (*Pm*) ring and the diphosphate side chain are excluded. For thiamin catalysis, the positive charge on the thiazolium nitrogen was generally assumed to attract excess electron density on carbanion

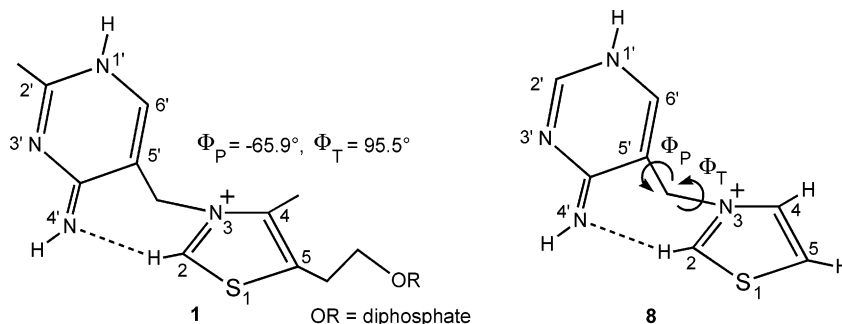
## SCHEME 1: Mechanism of Azolium C2–H Deprotonation as the Proton on C2 Moves toward an Arbitrary Base, B, To Form the Labeled Transition State (TS) and Ultimately Generates the Carbanion



intermediates and serve as what has been called the “electron sink.”<sup>8,9</sup> Contrary to this expectation our QTAIM analysis has shown that the quaternary N3 atom in the azolium rings, customarily assigned a formal charge of +1, turns out to bear more than one full negative charge in both the cations and ylidenes.<sup>7</sup> Among the heteroatom analogs containing sulfur, oxygen and nitrogen, only sulfur acts as an electron sink, literally gaining 0.38e in the ylide relative to the initial cation. These results lead us to pursue three questions that are fundamental to the structure–function relationship of thiamin.

The first question pertains to the uniqueness of sulfur. What is the basis of the ability of sulfur to play both thermodynamic and kinetic roles? Previously, the enhancement of the thermodynamic acidity of thiazolium ( $\text{p}K_{\text{a}} \sim 14$ ) over benzene ( $\text{p}K_{\text{a}} \sim 43$ ) was dissected by Streitwieser et al.<sup>10</sup> and shown to

\* Address correspondence to either author. E-mail: d.dupre@louisville.edu (D.B.D.), john.wong@louisville.edu (J.L.W.).

CHART 1: Thiamin Diphosphate V-Structure **1** in the Imino Form and Abbreviated Model Structure **8**<sup>a</sup>

<sup>a</sup> Note the proton on C2 is poised to form an intramolecular H-bond with imino N4' of the pyrimidine ring.

involve the azolium positive charge as the largest contributor ( $pK_a \sim 15.5$  units), followed by the aza effect ( $pK_a \sim 9.0$ ), and the thiophene sulfur effect ( $pK_a \sim 4.6$ ), which was not rationalized. Nor was there explanation given for the unusual acidity found for the thiazolium ions, including thiamin itself, in the range of  $pK_a = 17-19$ , as observed by H/D exchange in  $D_2O$  by  $^1H$  NMR.<sup>11</sup> Likewise, the equilibrium acidity estimated to be higher than  $pK_a = 16$  for thiamin models by direct titration in DMSO solution was not analyzed.<sup>12</sup> One stabilizing mechanism could be the polarizability of sulfur and of the bonds to sulfur as shown in the dithiane carbanions,<sup>13</sup> but this has not been demonstrated for the thiazolium. Stabilization by d-s orbital overlap was proposed by Haake et al.<sup>14</sup> to explain why H/D exchange in a thiazolium ion was 3000 times faster than imidazolium, but sulfur hypervalency in general was not supported in a later study by Reed and Schleyer.<sup>15</sup> Thus, the origin of the thermodynamic and kinetic effects of sulfur is still unclear. Schellenberger<sup>2</sup> has pointed out that, as the first step of the catalytic mechanism, the rate of carbanion formation determines the ultimate power ( $k_{cat}$ ) of all thiamin enzymes. Hence clarification of how sulfur works its unique role in thiamin is needed. Specifically, we will determine which orbitals are crucial to accepting the excess charge in the ylide and to forming the “electron sink” that stabilizes the transition state (TS) for C2 deprotonation.

The second question concerns the aminopyrimidine portion of thiamin. It is known that the dissociation rate (acidity) of the C2-H bond is enhanced by up to 4-6 orders of magnitude when ThDP is bound to enzyme.<sup>2</sup> This mechanism requires, as essential elements, a H-bond between the pyrimidine N1' and a glutamate side chain of the apoenzyme, as well as the obligatory albeit thermodynamically unfavored V-conformation of ThDP, as shown in Chart 1. This positions the 4'-amino group in functional contact with C2-H while allowing the energetically uphill conversion to the rare 1',4'-iminopyrimidine tautomer, as evidenced by spectroscopic measurements.<sup>16</sup> Recent molecular dynamics calculations, through the frequency of near attack H-bonding conformations, support the importance of the rare imino tautomer in the formation of the nucleophilic ylide.<sup>17</sup> This complex maneuvering appears to be too energetically expensive for forming just an internal base to abstract the proton from the C2 cation. We therefore wish to explore further whether there may be another compelling purpose such as electronic cooperation between the two ring components of thiamin in forming and stabilizing carbanion **1a**. It should be noted that the two ring  $\pi$ -systems are separated by a  $CH_2$  bridge that breaks conjugation. The rings can interact, however, via H-bonding between N4' and C2, as shown by the dashes in Chart 1.

The third question deals with the detection of the carbanion **1a**. In a perspective on thiamin enzymes, Jordan<sup>18</sup> notes that

invoking the presence of the unstable C2 carbanion in the proton-wire mechanism of ThDP-dependent enzymes proposed by Frank et al.<sup>19</sup> needs experimental proof, because an NMR study by Kern et al.<sup>20</sup> found no evidence that the cofactor acquires this carbanion before addition of the pyruvate substrate. The dilemma may be resolved by a mechanism in which a timed release of the carbanion is switched on upon the approach of pyruvate in the active site of the enzyme. This resolution would require understanding the energetics of C2, its deprotonation, and the switch that releases the carbanion. A variable H-bonding scheme between N4' and C2 may achieve this goal and hence is investigated herein.

In this study, the azolium models are broadened to include X-substitution by selenium, **5**, a larger heteroatom with lower electronegativity than sulfur, and also to include two dihydro derivatives, bearing one, **6**, or two  $\pi$ -bonds, **7**, in the five-membered ring. These models **2a-7a** (Scheme 1) allow a more complete analysis of the atomic size, electronegativity, and conjugation effects on carbanion formation at C2. Further, model **8**, extended now to comprise the 1',4'-iminopyrimidine functionality, mimics the enzyme bound thiamin V-structure **1** (Chart 1). Accordingly, deprotonated ThDP **1a** is modeled by **8a**. In terms of methodology to address the questions raised, quantitative charge distributions from the theory of atoms in molecules continue to serve the purpose. Particularly suited to the present tasks is natural bond orbital (NBO)<sup>21-23</sup> theory that makes possible quantitative comparisons of various localized hybrid orbitals in charge-transfer interactions and in the makeup of canonical molecular orbitals (CMOs)—particularly the frontier HOMO and LUMO.

## Methods

The equilibrium geometries of the molecules of this study are fully optimized, including normal-mode frequency analysis, using density functional theory (DFT) at B3LYP/6-31G(d,p),<sup>24,25</sup> as implemented in Gaussian03.<sup>26</sup> All the molecular structures labeled with bold letters are either stationary states on the potential energy surface with no imaginary normal-mode frequencies or transition states (TS) with exactly one imaginary frequency. The starting geometry for model **8** is based on the experimental, xyz-coordinates of the thiamin cofactor in the V-conformation reported by Dyda et al.<sup>27</sup> in their X-ray crystal structure of pyruvate decarboxylase (PDC). The molecule is completely relaxed, including the important torsional angles<sup>28</sup>  $\Phi_T = C2-N3-C-C5'$  (thiazol side) and  $\Phi_P = N3-C-C5'-C4'$  (pyrimidine side) about the methylene bridge connecting the two rings. The optimized coordinates of all models of this study are found in the Supporting Information for this paper.

The resultant electron density,  $\rho$ , obtained from the wave function of all optimized structures is analyzed with natural bond

orbital theory and the theory of atoms in molecules. NBO theory is useful in the interpretation of the electronic structure of molecules in terms of local, hybrid orbitals and their interactions—concepts familiar to chemists.<sup>21–23</sup> QTAIM theory<sup>5,6</sup> on the other hand analyzes the physical properties of the topology of the complete electron density of a molecule, providing a rigorous delineation of the size and three-dimensional shape of atoms within a molecule and the way they are bonded together.

In the NBO approach, the density matrix is transformed so as to provide maximal electron occupancies in a set of one-atom and two-atom centered hybrid orbitals with features of lone pairs,  $\sigma$ - and  $\pi$ -bonds. These Lewis orbitals are complemented by a set of higher energy, sparsely occupied Rydberg and antibonding  $\sigma^*$ - and  $\pi^*$ -orbitals. Charge-transfer interactions are evident in matrix elements connecting almost filled Lewis and the antibonding, non-Lewis orbitals. The H-bond, for example, is recognized in NBO theory as a general acid/base interaction, with a portion of the lone-pair electron density of the base,  $n(\text{B})$ , being delocalized into the  $\sigma^*(\text{A}-\text{H})$  antibonding orbital of the acidic proton donor.<sup>21–23</sup> In this view,  $n(\text{B}) \rightarrow \sigma^*(\text{A}-\text{H})$  is responsible for the H-bond. This interaction is assessed quantitatively in this work by use of second-order perturbation theory, where the energy lowering,  $E^{(2)}$ , due to the interaction of two localized orbitals  $a$  and  $b$  of energies  $E_a$  and  $E_b$ , respectively, is given by  $E^{(2)} = -2\langle a|F|b\rangle^2/(E_a - E_b)$ , where  $\langle a|F|b\rangle$  is the appropriate element of the one-electron Fock or Kohn–Sham matrix.<sup>23</sup> Recent progress<sup>29</sup> in NBO theory allows the decomposition of canonical molecular orbitals (CMOs) into a weighted set of underlying NBOs. In this manner one may clearly see the relative importance of various types of hybrid orbitals to the makeup of an overall CMO, particularly the frontier HOMO and LUMO. The NBO/CMO method available in NBO 5.0 is used for these calculations.<sup>29</sup>

QTAIM theory focuses on the properties of the topology of the electron density and its Laplacian  $\nabla^2\rho$ , obtained either by experiment or by calculation. In this analysis, an atom in a molecule is rigorously defined as a quantum mechanical entity bounded by a three-dimensional surface of zero flux in the gradient of  $\rho$ . A chemical bond between two atoms is distinguished by a path of maximal electron density between the nuclear attractors with a (3, -1) critical point (saddle point) on the interatomic surface (IAS) joining the two atoms. The properties of the bond critical point (BCP) serve to categorize different types of chemical bonds. The covalent bond generally manifests large values of the electron density,  $\rho(r_{\text{cp}})$ , at the BCP. The Laplacian,  $\nabla^2\rho(r_{\text{cp}})$ , is also generally large and negative at this point,<sup>5,6,30</sup> reflecting the dominance of contraction of electron density along the bond path (BP) in covalent bonds. In this case, the electronic charge is concentrated between nuclei and thus shared.

The total local energy density  $H_b = G(r_{\text{cp}}) + V(r_{\text{cp}})$  at a BCP reflects the balance between the local kinetic energy density  $G$  (always a positive quantity) and the local potential energy  $V$  (always a negative quantity).  $H_b$  is sometimes also quoted as a measure of covalency.<sup>31</sup> In a covalent bond,  $V(r_{\text{cp}})$  is always in excess and  $G(r_{\text{cp}})$  is small, making  $H_b$  negative—more so for a strong bond than a weak one. The degree of localization,  $\lambda(\text{A})$ , of electrons within the QTAIM-defined atomic basins and their delocalization,  $\delta(\text{A},\text{B})$ , into the basins of other atoms is also calculated as described by Fradera et al.<sup>32</sup> and Biegler-König and Schonbohm.<sup>33</sup> These calculations are based on integrations of the electron-pair density over individual atomic basins and between bonded and nonbonded atomic basins within the molecule. The indices provide a measure of electron-pair sharing

**TABLE 1: QTAIM Delocalization Indices  $\delta(\text{C2},\text{X})$  for C2 with Indicated Atoms or Groups of the Azolium Ylidene Models**

	2a X = S	3a X = O	4a X = NH
$\delta(\text{C2},\text{X})$			
C2 delocalized to			
X	1.31	0.95	1.10
N3	1.23	1.11	1.08
ring C, N, and X atoms	2.74	2.23	2.34
$\lambda(\text{C2})$ localization index	4.25	3.89	3.93

arising from exchange correlation by averaging the effect of following the spread of the Fermi hole—a region of exclusion of like-spin electron density of a representative electron that conversely results in pairing with another electron of opposite spin. Coulomb correlation is also introduced in our calculations through density functional theory. QTAIM analysis is performed with the AIM2000 program<sup>33</sup> using wave functions generated with the Gaussian electronic structure package.

## Results and Discussion

### Sulfur facilitates carbanion electron delocalization.

Table 1 lists the major QTAIM delocalization indices,  $\delta(\text{C2},\text{X})$ , of electrons in the C2 atomic basin with the other ring atoms of the azolium ylidene models **2a**, **3a**, and **4a** (fully optimized stationary states). The sulfur analog is found to exhibit the most advantage for delocalization stabilization by every measure of these indices. Despite the fact that the C2–X bond distance is the longest for X = S, the C2 delocalization (primarily the C2 lone-pair charge concentration) with sulfur is the largest with an index of 1.31. Also, participation of N3 ( $\delta = 1.23$ ) and the group of all ring carbons and heteroatoms ( $\delta = 2.74$ ) is maximal when X = S. The localization index  $\lambda(\text{C2})$  for the unshared  $\sigma$ -electrons at C2 is also the largest at  $\lambda = 4.25$  when X = S. These results show that sulfur is not limited to being an electron sink on its own but interacts constructively with other atoms to spread out charge. To understand this role better, we apply the methods of NBO/CMO theory to examine how sulfur facilitates this electron sink.

**Azolium LUMOs provide charge stabilization in the course of C2–H deprotonation.** The thiamin carbanion **1a** is a result of deprotonation to a general base, B, as represented in Scheme 1 for the azolium models **2–7**. This reaction involves a transition state (TS) with C2 bearing a nominal partial negative charge, resembling the ylidene product **2a–7a**. The developing electron density at C2 in the TS should reside in a LUMO akin to that of azolium ylidene. Hence the relative orbital contributions and energies of the LUMO and HOMO of these ylidenes are analyzed to evaluate the stability of the TS and the carbanion product. We are assuming here that the TS, where the azolium ring is H-bonded to an arbitrary base B, is in a late stage of proton transfer where the electronic structure of the five-membered ring (sans proton) is similar to that of the ylidene carbanion product. This will be proven for the TS of model **8** in more elaborate calculations in a later section of this paper.

Table 2 summarizes the results of the NBO/CMO analysis of the LUMO of the azolium ylidene models. From the numbers listed for fractional participation of the respective NBOs, it is clear that the  $\pi$ -system is crucial for accepting the negative charge developing at C2. The TS for production of the ylidene **2a** would exhibit the most uniform distribution of orbitals in the  $\pi$ -region, with  $\pi^*(\text{C2}=\text{N3})$  at 0.40,  $\pi^*(\text{C4}=\text{C5})$  at 0.36, and  $p\pi(\text{S})$  at 0.18—accounting for 94% of the LUMO. The corresponding CMO decomposition values for the starting cation

**TABLE 2: NBO/CMO Analysis of Relative, Fractional Orbital Contributions, and Energy (in au) of the LUMO of Azolium Ylidenes in Late Transition State Models of Thiamin Ylidene Formation**

thiazolium ylidene 2a X = S	conjugation variation dihydro analogs		electronegativity variation inductive analogs		
	6a X = S (4,5-dihydro)	7a X = CH <sub>2</sub>	3a X = O	4a X = NH	5a X = Se
$\pi^*(C2=N3)$	0.40	0.80	0.43	0.19	0.44
$\pi^*(C4=C5)$	0.36	n/a	0.40	0.60	0.78
$p\pi(X)$ lpr <sup>a</sup>	0.18	0.09	0.13		0.18
energy	-0.005	+0.008	-0.010	+0.020	+0.044

<sup>a</sup> lpr = lone pair.

**TABLE 3: Geometric Parameters of Azolium Ylidene Models (Bond Distances in Å; Bond Angles in Degrees)**

	2a	6a	7a	3a	4a	5a
	X = S	X = S (4,5-dihydro)	X = CH <sub>2</sub>	X = O	X = NH	X = Se
C2-X	1.740	1.729	1.524	1.371	1.371	1.891
C2-N3	1.353	1.322	1.332	1.359	1.372	1.349
C5-X	1.754	1.877	1.509	1.376	1.391	1.881
$\angle X-C2-N3$	104.7	109.0	107.2	102.9	100.7	104.1
$\angle C2-X-C5$	95.2	96.5	107.2	111.4	114.3	90.7
N3-C4	1.402	1.496	1.439	1.400	1.394	1.405

2 are similar in kind, but with weightings of 0.60, 0.06, and 0.23, respectively. It appears that the TS for **2** going to **2a** will have a LUMO that covers the entire  $\pi$ -region of the ring, with energy of -0.005 au.

Substituting the more electronegative oxygen atom or NH group for sulfur raises the  $\pi^*(C4=C5)$  NBO to dominance (0.60 for oxygen, 0.78 for NH) at the expense of the other two  $\pi, \pi^*$ -components. For X = NH, the other two orbitals fall below the analytical threshold of 0.05. The net effect of a more electronegative X is higher LUMO energies for **3a** (+0.020 au) and **4a** (+0.044 au), possibly due to a more limited  $\pi$ -space to accommodate the developing charge of the TS. A similar confinement to just one  $\pi^*$ -orbital is imposed in 4,5-dihydrothiazolium **6a**, where  $\pi^*(C2=N3)$  predominates in the TS, also raising energy to +0.008 au. However, the TS for another dihydro derivative, **7a**, a  $\beta$ -pyrrolium species with X = CH<sub>2</sub> that retains two  $\pi$ -bonds but lacks the sulfur lone pair, appears to fare as well as **2a**, with a LUMO energy of -0.010 au. This may be a coincidence of a favorable ring skeleton that offsets the loss of the  $p\pi$  orbital in **7a**. The geometric parameters of the azolium models are shown in Table 3. Note that the three carbon bonds emanating from X and C2 in **7a** are shorter than those of **2a**. Also, the two bond angles in **7a** containing C2 or X are less acute than those of **2a**, making its  $\sigma$ -bonds stronger. However, the significantly longer N3-C4 bond (1.439 vs 1.402) argues for less extended  $\pi$ -conjugation.

The interplay of electronegativity  $\chi$  and atomic size with bond strength and  $\pi$ -conjugation is a balancing act. This can be seen in the comparison of models **2a** and **5a**. The fourth period selenium atom ( $\chi = 2.4$ ) is less electronegative than the third period sulfur ( $\chi = 2.5$ ). For the selenium model **5a**, the two single bonds of X are substantially longer than those of the sulfur analog (1.891 and 1.881 vs 1.740 and 1.754 Å, respectively). The C2-X-C5 bond angle is more acute (90.7° vs 95.2°), whereas the C2-N3 and N3-C4 bond lengths, and the bond angle at C2 are relatively unchanged. The  $\pi$ -orbital overlap between selenium and its neighbors is also less than that of sulfur. This difference is seen in the orbital overlap contours of sulfur and selenium with the C2 edge of the  $\pi^*(C2=N3)$  antibond illustrated in Figure 1. Indeed from NBO calculations, we find that the  $E^{(2)}$  interaction energies

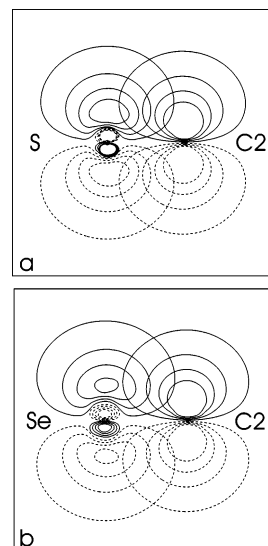


**Figure 1.** Contour plots of  $\pi$ -orbital overlap of sulfur (a) and selenium (b) with the C2 edge of the  $\pi^*(C2=N3)$  natural bond orbital in azolium ylidene models **2a** and **5a**. The overlap is greater for the sulfur analog (e.g., the outermost contour of C2 extends into the innermost contour of the outer lobe of sulfur, but not of selenium). Four contours are shown for each atom. The outermost contour roughly corresponds to the van der Waals radius of the atom and has a value of  $\pm 0.03$  au. The increment between contours is  $\pm 0.05$  au.

**TABLE 4: NBO/CMO Analysis of Relative, Fractional Orbital Contributions, and Energy (in au) of the HOMO of Azolium Ylidene Models**

thiazolium ylidene 2a X = S	conjugation variation dihydro analogs		electronegativity variation inductive analogs		
	6a X = S (4,5-dihydro)	7a X = CH <sub>2</sub>	3a X = O	4a X = NH	5a X = Se
$\sigma(C2)$ lpr <sup>a</sup>	0.81	0.78	0.83	0.84	0.74
$\sigma(C2-X)$	0.09	0.08	0.07		0.16
energy	-0.216	-0.210	-0.188	-0.220	-0.198

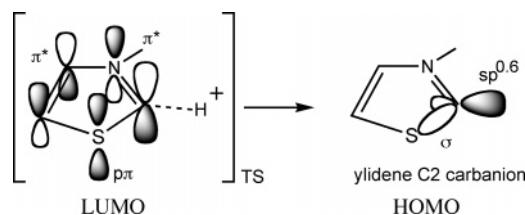
<sup>a</sup> lpr = lone pair.

for  $n(X) \rightarrow \pi^*(C2=N3)$  are 27.3 kcal/mol for X = Se and 35.4 kcal/mol for X = S. Overall, the net result of this interplay of  $\chi$  and atomic size when selenium replaces sulfur is that there is little change in the LUMO makeup and energy from the thiazolium ylidene (Table 2).

#### Azolium HOMOs participate in carbanion stabilization.

Table 4 lists the results of our NBO/CMO analysis of the effect of the HOMO on carbanion stability in the azolium ylidenes **2a** to **7a**. These HOMOs are found to be constituted from  $\sigma$ -orbitals with the  $\sigma(C2)$  lone-pair predominant. Previously,<sup>7</sup> our calculations with QTAIM theory of the Laplacian of the electron density of C2 in the thiazolium ylidene showed that this atom exhibits distinct lone-pair concentration of charge in the  $\sigma$ -plane. The additional contribution of the  $\sigma(C2-X)$  NBO found here is strongest for the least electronegative selenium atom (0.16), falling below threshold for the most electronegative NH and oxygen substitutions. However, this pattern cannot be correlated with the HOMO energies, which range from about -0.19 au for **7a** (X = CH<sub>2</sub>) to about -0.22 for **2a** (X = S) and **3a** (X = O), but reflects multifactorial influences. One message stands out: sulfur provides a reasonable compromise between effects of electronegativity and atomic size. Replacing sulfur by the smaller but more electronegative NH group or oxygen atom as X would impair the LUMO effectiveness as an electron sink. Furthermore, the use of selenium in place of sulfur would lead to a five-membered ring geometry less fit for aromatic

**SCHEME 2: Depiction of Orbital Contributions to the LUMO of the TS and the HOMO of the Thiazolium Ylidene Product 2a**



conjugation. Because deprotonation of C2–H can only occur in a stable molecule like the aromatic thiazolium ring, the two dihydro derivatives can be dismissed: **6a** would be too readily dehydrogenated to regain conjugation and **7a** is actually the extremely rare form of pyrrole  $\beta$ -protonation. Thus, the thiazolium deprotonation summarized in the orbital picture in Scheme 2 yields the best TS and carbanion product **2a** because of the low electronegativity and moderate size of the sulfur atom.

**The effectiveness of sulfur as the electron sink is not due to hypervalency.** Sakaki et al.<sup>34</sup> also recognized that sulfur, not nitrogen, would be the source of the electron sink in the thiazolium moiety of thiamin. They speculated that introducing extravalent orbitals on the sulfur atom could hold excess electrons. However, no evidence for such hypervalency was found in a similar study by Reed and Schleyer.<sup>15</sup> Our NBO analysis demonstrates that the sulfur atom in the thiazolium ylidene has a natural atomic orbital population of [core]3s(1.65)-3p(3.90)4s(0.01)3d(0.03)4p(0.01), with very little electronic density in the extravalent 4s, 3d, and 4p orbitals. Selenium in **5a** also has very low electron population in 5s, 4d, and 5p states, with an electron configuration of [core]4s(1.72)4p(3.78)5s(0.01)-4d(0.02)5p(0.01).

**Relay of LUMO stabilization from thiazolium to pyrimidylimine occurs in the deprotonation pathway.** Recent studies<sup>35,36</sup> have shown that enzyme-bound thiamin adopts a V-shaped conformation **1** with 4'-pyrimidylimine adroitly placed in the vicinity of the thiazolium ring and capable of forming an intramolecular H-bond with C2–H. Thus, the two ring systems separated by the CH<sub>2</sub> bridge can interact via H-bonding between N4' and C2. The X-ray structure of the pyruvate decarboxylase–thiamin complex shows the thiamin torsional angles about the bridging methylene group to be  $\Phi_T = 95.5^\circ$  and  $\Phi_P = -65.9^\circ$ .<sup>27</sup> This unique structure is necessary for the deprotonation of **1** to form **1a**. To extend our study to more realistic models, we adopt structure **8**, shown in Chart 1, to mimic **1**. This thiamin model eliminates the diphosphate side chain (not thought to be a part of the catalytic activity of the enzymatic cofactor) and replaces the methyl groups on C4 and C2' with hydrogens.

To follow the deprotonation process, we incrementally transfer H<sup>+</sup> from C2 to the 4'-imine nitrogen (denoted here as N4') in steps of 0.05 Å. At each point along the path, the transient state of the V-structure model is optimized under the sole constraint of the fixed C2–H<sup>+</sup> bond distance at the given increment. The results are plotted in Figure 2 as the change of energy,  $\Delta E$ , across the reaction coordinate. The TS, **8TS**, is found at point 6 and the C2 ylidene product, **8a**, at point 12. Note that point 6 is indeed a late TS with the proton being well along the path to produce the ylidene carbanion. NBO/CMO analysis is performed on each of the structures at the labeled points 1 through 12. The results are listed in Tables 5 (path A to TS) and 6 (path B to carbanion product) and shown graphically for the more revealing transient structures in Chart 2A–D. In this model, we consider only the *direct* transfer

of the proton from C2 to N4'. If the enzyme involves a water molecule in the deprotonation process, a different, perhaps higher activation energy barrier may occur, as suggested in the calculations of Lie et al.<sup>17</sup>

The LUMO composition of cation **8** at the starting point (pt 1) (Table 5) is almost identical to that of the TS to the thiazolium ylidene **2a** (compare Scheme 2 and Chart 2A). Thus, the developing negative charge at C2 of **8** should be similarly stabilized in the LUMO right from the start of deprotonation. This stabilization mode continues onto point 4 (Table 5), at which point divergence from the TS composition of **2a** occurs—as seen in the LUMO in Chart 2B, which is composed of contributions from both ring systems. Although there are still contributions of 0.40 from  $\pi^*(C2=N3)$  and 0.14 from  $p\pi(S)$  from thiazolium (Table 5), the  $\pi^*(C4=C5)$ , significant in **2a** (Table 2), is being replaced by  $\pi^*(C4'=N4')$  and  $\pi^*(C5'=C6')$  from the pyrimidylimine side. This trend is accentuated at point 5, with the disappearance of  $p\pi(S)$  and  $\pi^*(C2=N3)$ . Here some contribution from  $\pi^*(C2'=N3')$  emerges (Table 5 and Chart 2B). Note that the LUMO energy at point 4 has peaked, although the activation energy is still rising, until point 6, which is designated the TS, as shown in Figure 2. Only  $\pi$ -orbitals of the pyrimidylimine ring make up the LUMO of the TS at point 6 (Chart 2C). The gradual decline of LUMO energy after point 4 coincides with increasing contributions from pyrimidylimine  $\pi^*$ -orbitals and  $p\pi(N1')$  as deprotonation moves forward to the TS at point 6 and to the carbanion at point 12 (Tables 5 and 6). The thiazolium orbitals are disappearing under the reporting threshold after point 4 as noted in the tables. Thus, the V-structure in model **8** has established a relay of electron sinks in the LUMOs (across Tables 5 and 6) from thiazolium to pyrimidylimine, to accept the developing negative charge at C2. The result is a substantial drop of LUMO energy, from  $-0.01$  for thiazolium ylidene **2a** to  $-0.20$  au for the more complete model **8a**.

**Relay of HOMO stabilization from pyrimidylimine to thiazolium occurs in the deprotonation pathway.** The HOMO picture is different but supportive of the stabilizing picture of the LUMOs. The major contributions to the HOMO shift from  $\pi$ -orbitals of pyrimidylimine at the start (Chart 2A and Table 5) to  $\sigma$ -orbitals of thiazolium at the end of deprotonation (Chart 2D and Table 6). From points 1 to 4, the HOMOs encompass only the pyrimidylimine  $\pi$ -system. These contributions diminish rapidly after the TS is reached, and are almost negligible after point 8. Meanwhile the  $\sigma$ -orbitals become dominant, especially  $\sigma(C2)$  lone pair, which is supplemented by  $\sigma(C2-S)$ ,  $\sigma(N4'-H^+)$ , and  $\sigma^*(N4'-H^+)$ . Two significant stabilizations are noted: the HOMO of **8a** ends up as  $\sigma$ -orbitals to accommodate the C2 lone pair—the same contribution that supports the thiazolium ylidene **2a**; the contribution by the  $\sigma^*(N4'-H^+)$  antibond suggests the carbanion can also delocalize through a  $n\sigma(C2) \rightarrow \sigma^*(N4'-H^+)$  H-bonding interaction as shown in Chart 2D.

**Operation of H-bonding scheme in the thiamin V-structure allows the formation of cryptic C2-carbanion.** The N4'...H<sup>+</sup>...C2 H-bond alluded to above imposes a distance requirement between C2 and N4' that is favored in specific V-structures of thiamin. The thiamin V-conformation is rare in solution of free thiamin, which prefers non-V forms such as F and S.<sup>37,38</sup> The V, F, and S forms are classifications of crystal conformations of free and enzyme-bound thiamin and derivatives.<sup>37,38</sup> Their distinctions concern the torsional angles  $\Phi_T$  and  $\Phi_P$  at the  $-CH_2-$  bridge: the V form has  $\Phi_T = \pm 90^\circ$  and  $\Phi_P = \pm 90^\circ$ ; the F form,  $\Phi_T = 0^\circ$  and  $\Phi_P = \pm 90^\circ$ ; and the S form,

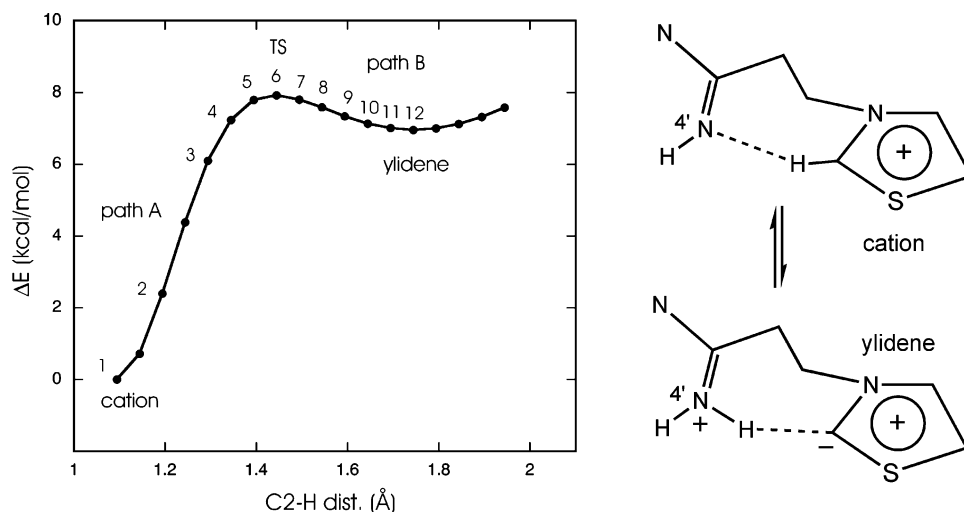


**Figure 2.** Energy changes,  $\Delta E$ , along the reaction coordinate for proton transfer across the V-structure from the thiazolium cation to the imino nitrogen N4', producing the ylidene carbanion product. The structure at point 6 is the (late) transition state (TS). Path A extends from the cation (point 1) to the TS (point 6). Path B carries the model from the TS to the ylidene (point 12).

**TABLE 5. NBO/CMO Analysis of Relative, Fractional Orbital Contributions, and Energies (in au) of the HOMO and LUMO in **8** as It Approaches (Path A) the Transition State for Proton Transfer from the Cation (Pt. 1) to the *Pm* System of the V-Structure<sup>a</sup>**

	path A					
	pt. 1 (start)	pt. 2	pt. 3	pt. 4	pt. 5	pt. 6 (TS)
C2–N4'	2.888	2.819	2.696	2.652	2.627	2.621
C2–H+	1.094	1.194	1.294	1.344	1.394	1.444
N4'–H+	2.041	1.768	1.479	1.370	1.289	1.229
$\angle$ C2–H–N4'	131.8	143.5	152.9	155.4	156.7	157.2
$\Phi_T$	79.9	65.9	61.0	60.5	61.0	62.0
$\Phi_P$	–75.5	–74.9	–70.8	–69.0	–67.8	–67.2
HOMO						
$\pi(C4'=N4')$	0.34	0.33	0.31	0.29	0.23	0.19
$\pi^*(C4==N4')$	0.08	0.08	0.09	0.09	0.07	0.06
$\pi(C5'=C6')$	0.22	0.22	0.23	0.23	0.21	0.17
$\pi(C2'=N3')$	0.12	0.11	0.10	0.09	0.08	0.06
$p\pi(N1')$ lpr	0.18	0.18	0.17	0.16	0.15	0.11
$\sigma(N4')$ lpr $sp^{2.0}$					0.06	
$\sigma(C2)$ lpr $sp^{1.6}$						0.19
$\sigma(C2-H+)$					0.08	
energy	–0.352	–0.359	–0.371	–0.377	–0.381	–0.384
LUMO						
$\pi(C4=C5)$	0.05	0.05				
$\pi^*(C4=C5)$	0.07	0.08	0.08			
$\pi^*(C2=N3)$	0.58	0.58	0.56	0.40		
$\pi^*(C2'=N3')$					0.10	0.05
$\pi^*(C4'=N4')$				0.12	0.16	0.24
$\pi^*(C5'=C6')$				0.10	0.53	0.49
$p\pi(S)$ lpr	0.22	0.22	0.21	0.14		
$p\pi(N1')$ lpr						0.07
energy	–0.210	–0.202	–0.188	–0.182	–0.184	–0.188

<sup>a</sup> Geometric parameters are included: distances in Å, angles in degrees.

$\Phi_T = \pm 100^\circ$  and  $\Phi_P = \pm 150^\circ$ . Inspection of unoptimized, rigidly rotated models of **8** shows that only certain V-conformations can produce reasonable distances to sustain H-bonding between C2 and N4'. The C2–N4' distances for V(+,–) and V(–,+) conformers are 3.4–3.5 Å—close enough for H-bonding. On the other hand, V(+,+) and V(–,–) conformers produce distances of 4.7–4.8 Å; the F(0,±) conformers, 3.7–3.8 Å; and S(±,±), 4.8–5.3 Å. Experimentally, the enzyme-bound thiamin is found to be the V(+,–) structure in pyruvate decarboxylase.<sup>27,37,39</sup> As seen in Tables 5 and 6, the structural optimization of model **8** produces a favorable H-bonding system, with a C2–N4' distance of 2.888 Å,  $\angle$ C2–H–N4' angle of 132°, and torsional angles ( $\Phi_T$ ,  $\Phi_P$ ) of 79.9°, –75.5°. In the TS, the corresponding data are 2.621

Å, 157°, and 62.0°, –67.2°, respectively—values indicative of an even stronger H-bond. In the ylidene, these values are 2.751 Å, 153°, and 69.6°, –68.8°, respectively. The torsional angles ( $\Phi_T$ ,  $\Phi_P$ ) of thiamin model **8** remain within the confines of the V-structure throughout the simulated proton transfer depicted in Chart 2 and described in Tables 5 and 6.

A similar message favoring the H-bonding scheme is given by the NBO  $E^{(2)}$  values of the respective H-bonding interactions. This measure of the relative strength of the H-bond is 172 kcal/mol at the TS, vs 10 kcal/mol found for the H-bond in **8** and 57 kcal/mol in **8a**—indicating a strong H-bond in the TS to anchor the developing carbanion at C2. NBO analysis also reveals that in the TS there is a three-center, four-electron bond across N4'⋯H<sup>+</sup>⋯C2, containing 3.90e with equal contributions

**TABLE 6: NBO/CMO Analysis of Relative, Fractional Orbital Contributions, and Energies (in au) of the HOMO and LUMO in **8** after the TS (Path B), Completing Proton Transfer to N4' (Pt. 12) of the *Pm* System in the V-Conformation<sup>a</sup>**

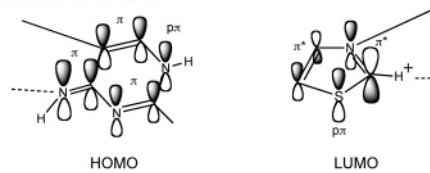
	path B					
	pt. 7	pt. 8	pt. 9	pt. 10	pt. 11	pt.12 (product)
C2–N4'	2.628	2.643	2.664	2.691	2.720	2.751
C2–H+	1.494	1.544	1.594	1.644	1.694	1.744
N4'–H+	1.186	1.153	1.128	1.109	1.093	1.080
∠C2–H–N4'	157.1	156.7	156.1	155.2	154.2	153.1
Φ <sub>T</sub>	63.3	64.6	65.9	67.2	68.5	69.6
Φ <sub>P</sub>	-66.9	-67.0	-67.2	-67.6	-68.2	-68.8
HOMO						
π(C4'=N4')	0.12	0.07				
π*(C4'=N4')						
π(C5'=C6')	0.11	0.07				
π(C2'=N3')						
π(C4=C5)	0.06	0.06				
pπ(N1') lpr	0.07					
σ(C2) lpr	0.33	0.42	0.53	0.61	0.66	0.68
σ(N4'–H+)	0.06	0.07	0.06	0.06	0.06	0.06
σ*(N4'–H+)		0.06	0.06	0.06	0.06	0.06
σ(C2–S)			0.06	0.06	0.07	0.07
energy	-0.384	-0.383	-0.381	-0.379	-0.377	-0.375
LUMO						
π(C2'=N3')	0.06	0.07	0.07	0.07	0.08	0.08
π*(C4'=N4')	0.31	0.36	0.39	0.41	0.42	0.43
π(C5'=C6')		0.05	0.06	0.06	0.07	0.07
π*(C5'=C6')	0.42	0.35	0.31	0.28	0.26	0.24
pπ(N1') lpr	0.09	0.11	0.12	0.13	0.13	0.14
energy	-0.191	-0.194	-0.197	-0.199	-0.201	-0.203

<sup>a</sup> Geometric parameters are included: distances in Å, angles in degrees.

from the σ(N4'–H<sup>+</sup>) bond and the nσ(C2) sp<sup>1.6</sup> lone-pair orbitals.

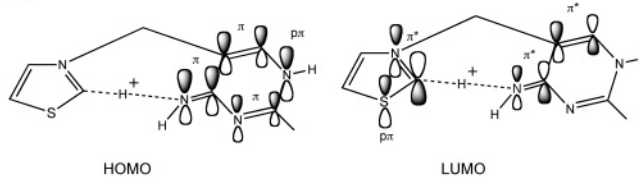
We also analyze this H-bonding effect on C2–H deprotonation by QTAIM theory. First, the QTAIM delocalization indices are determined for the TS, **8TS**, to **8a**. The indices calculated for C2 electron-pair sharing with sulfur and N3 are 1.36 and 1.23, respectively, and the C2 localization index is 4.09. These values are comparable to those observed for the thiazolium ylidene model **2a** (cf. Table 1). Significant delocalizations of C2 electron density to H<sup>+</sup> (0.33) and N4' (0.16) of the H-bond are also indicated, supporting the postulate that this H-bond stabilizes the C2 lone pair. Next, the influence of the intramolecular H-bond formed in the TS is shown by the Laplacian contour plot of the electron density in Figure 3A. The darker lines represent regions of charge concentration that clearly demonstrate a large and continuous accumulation of electron density on both sides of the bridging proton. The covalent character of this three-center H-bond in the TS is seen in the properties listed in Table 7 for the two bond critical points between C2 and H<sup>+</sup> and N4' and H<sup>+</sup>. The relatively large values of ρ(r<sub>cp</sub>) and the negative values of ∇<sup>2</sup>ρ(r<sub>cp</sub>) and H<sub>b</sub> are indicative of covalent character in both the bonds. The N4'–H<sup>+</sup> bond is clearly stronger, but C2–H<sup>+</sup> also exhibits a sizable and negative value of ∇<sup>2</sup>ρ(r<sub>cp</sub>). This H-bond thus exerts an anchoring effect on the V-structure at the TS along the proton-transfer coordinate.

With respect to the ylidene **8a**, the Laplacian plot in Figure 3B shows the accumulation of shared charge between N4' and the proton, but a gap of charge depletion (green contour lines) between C2 and H<sup>+</sup>. Table 7 also compares the properties of this intramolecular H-bond in the ylidene product. The latter data show that the N4'–H bond is covalent—more so than that of N4'–H in the TS. The C2···H<sup>+</sup> bond, however, has a low value of ρ(r<sub>cp</sub>) and a low and positive value of ∇<sup>2</sup>ρ(r<sub>cp</sub>). This,

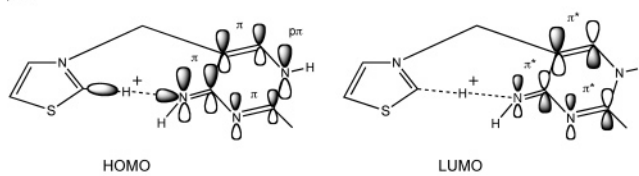
**CHART 2: Development of Orbital Contributions in the V-Structure along the C2–H<sup>+</sup> Path for Proton Transfer**A. Starting thiamin model **8** at pt. 1

B. Pre-TS transient structures showing significant changes in LUMO composition at:

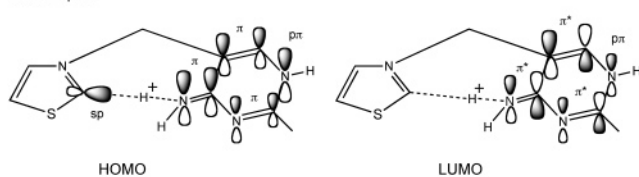
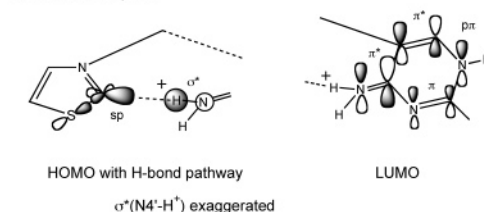
pt. 4



pt. 5



C. TS at pt. 6

D. Ylidene **8a** at pt. 12

along with the low, negative value of H<sub>b</sub>, is indicative of a normal H-bond with closed-shell interaction.

According to Figure 2, the ylidene **8a** has a mere 1 kcal/mol activation barrier to reverse the proton to cation **8**, whereas the forward reaction requires about 8 kcal/mol. Because the energy of **8a** is also about 7 kcal/mol higher than that of **8**, kinetic and thermodynamic production of the carbanion is highly unfavorable. This is in accord with the NMR study using <sup>13</sup>C2–thiamin diphosphate (δ(C2) = 155 ppm) by Kern et al.<sup>20</sup> This signal was just the same in thiamin as that found in the thiamin–enzyme complex; thus they concluded that the enzyme-bound thiamin does not exist as a discrete carbanion in detectable amounts but rather prevails in its protonated form. What if this ylide carbanion should exist as a carbene? Arduengo et al.<sup>40</sup> have shown that, for a crystalline thiazolium carbene, the C2 resonance of δ = 254 ppm was prominent. Upon formation of an olefin dimer, the resonance shifted dramatically upfield by 108 ppm. None of these new signals were detected in the enzyme-bound thiamin <sup>13</sup>C NMR study, rendering a carbenoid explanation of the thiamin carbanion unlikely. Thus, the present documentation of a H-bonding scheme, from N4'···H–C2 to N4'–H···C2, is a new proposition for a kinetic catalysis pathway: one that offers a practical means to form and conserve

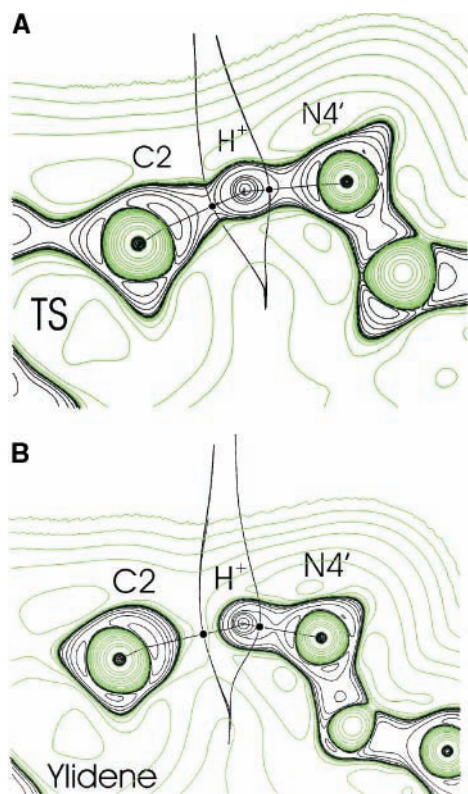


**Figure 3.** (A) Contour plot of the Laplacian of the electron density across the intramolecular H-bond in the deprotonation transition state, **8TS**, of the V-structure model **8**. Dark lines delineate regions of charge concentration; green lines map regions of charge depletion. Bond paths connecting the nuclei and the projection of the interatomic surface about  $H^+$  in the  $C2-H^+-N4'$  plane are also shown by thin dark lines. The small dark circles locate the two bond critical points at the bonding edge of the interatomic surface of  $H^+$ . (B) Contour plot of the Laplacian of the electron density across the intramolecular H-bond in **8a**, the ylidene carbanion of the V-structure model **8**.

**TABLE 7: QTAIM Properties (in au) of the Intramolecular H-Bonds Across the V-Conformer of Model 8 in the Deprotonation TS (8TS) and Product Ylidene Carbanion 8a**

BCP	TS		ylidene carbanion	
	$N4'-H$	$C2-H$	$N4'-H$	$C2-H$
$\rho(r_{cp})$	0.186	0.120	0.278	0.059
$\nabla^2\rho(r_{cp})$	-0.565	-0.123	-1.388	+0.060
$G_b$	0.065	0.041	0.052	0.028
$V_b$	-0.272	-0.112	-0.452	-0.042
$H_b = G_b + V_b$	-0.206	-0.071	-0.400	-0.013

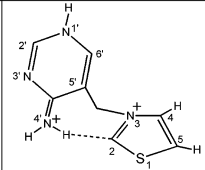
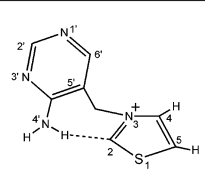
the C2 carbanion, but not accumulating it due to the 1 kcal/mol energy barrier for reversion.

In contrast to this work, a recent theoretical study of the catalytic mechanism of ThDP-dependent pyruvate decarboxylase,<sup>41</sup> the deprotonation of C2 was calculated to be *exothermic* by 18 kcal/mol, with very low activation energy barrier. In their models, where an abbreviated glutamate residue was contiguous to  $N1'$ , the proton associated with  $N1'$  had been transferred to the glutamate oxygen, producing consequences considerably different from those of our protonated  $N1'-H$  models on the intramolecular  $N4'-H\cdots C2$  interaction. The important and variable torsional angles,  $\Phi_T$  and  $\Phi_P$ , were also held frozen (apparently, erroneously, to ensure the maintenance of the necessary V-structure) in their calculations—thus precluding observation of many of the relaxation features discussed in this Article. But their conclusion that “the ylide formation is

**TABLE 8: Physical Properties of Molecule 8a before and after Deprotonation of  $N1'$  and Changes in Topological Properties of the  $N4'-H\cdots C2$  H-Bond (Distances in Å, Angles in Degrees, QTAIM Properties in Atomic Units)**

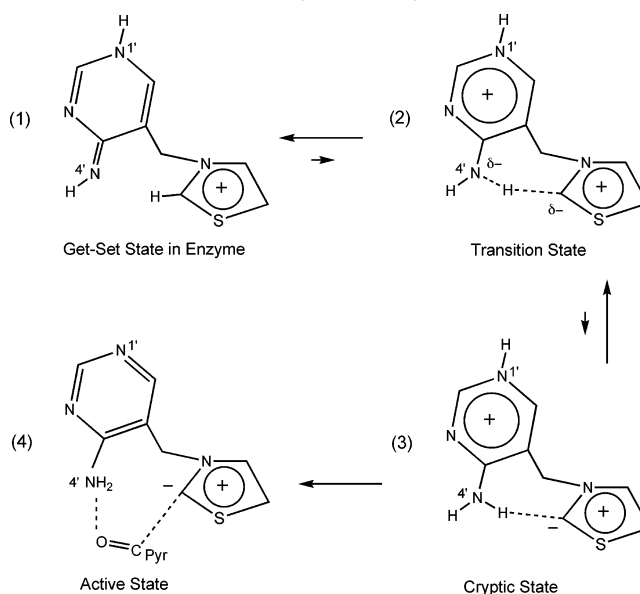
1. Geometry <sup>a</sup>	With $N1'H$	Without $N1'H$
$N4'-H$	1.080	1.027
$C2\cdots H$	1.744	2.051
$C2\cdots N4'$	2.751	2.983
$\Phi_{T,P}$	69.6, -68.8	86.1, -71.7
$\angle N4'HC2$	153.1	149.6

2. QTAIM properties of the $C2\cdots H$ bond		
$\rho(r_{cp})$	0.059	0.029
$\nabla^2\rho(r_{cp})$	0.060	0.058
$H_b = G(r_{cp}) + V(r_{cp})$	-0.013	-0.002

<sup>a</sup> Both models fully optimized with no constraints.

**SCHEME 3: Four Stages of the Initial Deprotonation Mechanism of ThDP-Enzyme Catalysis**



thermodynamically favorable and kinetically facile” is untenable in view of the NMR study<sup>20</sup> noted above.

**$N1'-H$  deprotonation is a switch for C2 carbanion release.** Given that this intramolecular H-bonding scheme sequesters a cryptic C2 carbanion, how then can C2 chemically act as a nucleophile? The clue may lie in the H-bonding strength of  $N4'-H\cdots C2$  that can be controlled by the state of protonation at  $N1'$ . Data in Table 8 compares the physical properties of these H-bonds with and without protonation of  $N1'$ . As seen in geometric and QTAIM properties, the  $C2\cdots H$  bond is significantly weakened by the absence of  $N1'$  protonation. Note that the bond length of  $C2\cdots H$  is about 20% longer, with the total energy  $H_b$  at the bond critical point being less than 1/6th as large. Additionally, the  $C2\cdots H$  bond will be physically disturbed by the approaching substrate. Starting with  $\Phi_T = 70^\circ$  and  $\Phi_P = -69^\circ$  for the ylidene **8a** (point 12, Table 6), these torsional



angles will undergo a considerable twist to accommodate the thiamin–pyruvate adduct. For example, the corresponding angles in the hydroxypyruvate–thiamin–transketolase complex, as measured by X-ray diffraction, are  $\Phi_T = 95^\circ$  and  $\Phi_P = -56^\circ$ .<sup>42</sup> The pyruvate substrate may activate the thiamin–enzyme complex by (1) triggering N1'–H dissociation (with the proton going back to the nearby glutamate side chain) and (2) imposing a torsional conformational change (even though remaining in the general V-structure zone). These actions are plausible in light of the pyruvate decarboxylase crystal structural analysis that has shown a cysteine residue, greater than 20 Å away from the ThDP site, is the most likely site of substrate activation.<sup>39</sup> A sequence of residue perturbations and movements were invoked to propagate the cysteine–pyruvate binding effects. Such motions may initiate the above H-bonding switch. Overall, the presence of the substrate results in a weakening and displacement of the H-bond involving C2—freeing the cryptic carbanion for nucleophilic addition.

## Conclusions

We have probed the origin of electron sinks in thiamin and the stabilization of its carbanion. Both the QTAIM delocalization indices of C2 in azolium ylidene models (X = S, O, NH) and NBO analysis reveal that the  $\pi$ -system is crucial for accepting the developing charge at C2. Sulfur gives the best orbital contributions to the LUMO of the TS and the HOMO of the thiazolium ylidene because of the low electronegativity and moderate size of the sulfur atom.

Two electron sinks working in tandem via an intramolecular H-bond are shown to be operative across the reaction coordinate of the thiamin V-structure model **8** as  $H^+$  is incrementally transferred from C2 to N4'. The NBO/CMO analysis shows that the developing charge at C2 of **8** from points 1 to 4 is stabilized in the LUMO just as in the thiazolium model. This is the first electron sink. Then the  $\pi$ -system of pyrimidylimine makes up the bulk of the LUMO going forward. The gradual decline of LUMO energy after point 4 coincides with increasing contributions from the second electron sink, mainly the pyrimidylimine  $\pi^*$ -orbitals and  $p\pi(N1')$ , as deprotonation moves past the TS. The HOMO picture is supportive of the LUMO conclusion. The HOMO of **8a** ends up as  $\sigma$ -orbitals to accommodate the C2 lone pair, the same contribution that supports the thiazolium ylidene **2a**. Furthermore, the presence of the  $\sigma^*(N4'-H^+)$  antibonding contribution suggests the carbanion can also delocalize through a  $n\sigma(C2) \rightarrow \sigma^*(N4'-H^+)$  H-bonding interaction.

An intramolecular H-bonding scheme is shown by geometric, NBO, and QTAIM analysis that allows C2–H activation without accumulating the unstable carbanion. Thus, once the C2 hydrogen is put into play by the proper V-structure, the H-bonding Scheme 3 provides for the kinetic catalysis to generate the rare carbanion that remains H-bonded. Complete deprotonation results only upon the arrival of an activating substrate like pyruvate that ultimately consumes the carbanion nucleophile. Thus we propose that the initial deprotonation of C2 in ThDP catalysis proceeds in four stages. In stage 1, ThDP is positioned on the enzyme in the V-structure as the iminopyrimidine tautomer as evidenced spectrally<sup>16</sup> in a “get-set” state. In stage 2, an intramolecular H-bond bridging the two  $\pi$ -systems has moved to a transition state for proton transfer. In stage 3, the C2 carbanion in a cryptic state is shielded by the intramolecular H-bond. In stage 4, the C2 carbanion is in the active state for attacking the pyruvate substrate. The active state is switched on by the N1' proton returning to the nearby glutamate residue and a torsional change at the bridging methylene group.

The latter effect is induced by the physical presence of substrate in the enzymatic channel.

**Acknowledgment.** Supercomputer time allocations received from the National Computational Science Alliance and from the Advanced Biomedical Computing Center of the Frederick Cancer Research and Development Center, National Institutes of Health, are acknowledged. Support for this work also came from a Research Initiation Grant from the Office of the Vice President for Research, University of Louisville, and an Intramural Research Grant from the College of Arts and Sciences, University of Louisville.

**Supporting Information Available:** Atomic coordinates of optimized structures **2a–7a**, **8**, **8a**, and **8TS**. Complete author list for ref 26. This material is available free of charge via the Internet at <http://pubs.acs.org>.

## References and Notes

- (1) Kluger, R. *Chem. Rev.* **1987**, *87*, 863–876.
- (2) Schellenberger, A. *Biochim. Biophys. Acta* **1998**, *1385*, 177–186.
- (3) Jordan, F. *Nat. Prod. Rep.* **2003**, *20*, 184–201.
- (4) Sprenger, G. A.; Phol, M. *J. Mol. Catal. B: Enzymatic* **1999**, *6*, 145–159.
- (5) Bader, R. F. W. *Atoms in molecules. A quantum theory*; Clarendon Press: Oxford, U.K., 1990.
- (6) Popelier, P. *Atoms in molecules. An introduction*; Prentice Hall: New York, 2000.
- (7) DuPré, D. B.; Wong, J. L. *J. Phys. Chem. A* **2005**, *109*, 7606–7612.
- (8) Voet, D.; Voet, J. G. *Biochemistry*, 3rd ed.; John Wiley: New York, 2004.
- (9) Nelson, D. L.; Cox, M. M. *Lehninger Principles of Biochemistry*, 3rd ed.; Worth: New York, 2000.
- (10) Streitwieser, A., Jr.; Scannon, P. J. *J. Amer. Chem. Soc.* **1973**, *95*, 6273–6276 and pertinent references cited therein.
- (11) Washabaugh, M. W.; Jencks, W. P. *Biochemistry* **1988**, *27*, 5044–5053.
- (12) Bordwell, F. G.; Satish, A. V. *J. Am. Chem. Soc.* **1991**, *113*, 985–990.
- (13) Xie, L.; Bors, D. A.; Streitwieser, A., Jr. *J. Org. Chem.* **1992**, *57*, 4986–4990.
- (14) Haake, P.; Bausher, L. P.; Miller, W. B. *J. Am. Chem. Soc.* **1969**, *91*, 1113–1119.
- (15) Reed, A. E.; Schleyer, P. v. R. *J. Am. Chem. Soc.* **1990**, *112*, 1434–1445.
- (16) Jordan, F.; Nemeria, N. S. *Bioorg. Chem.* **2005**, *33*, 190–215.
- (17) Lie, M. A.; Celik, L.; Jorgensen, K. A.; Schiott, B. *Biochemistry* **2005**, *44*, 14792–14806.
- (18) Jordan, F. *Science* **2004**, *306*, 818–820.
- (19) Frank, R. A. W.; Titman, C. M.; Pratap, J. V.; Luisi, B. F.; Perham, R. N. *Science* **2004**, *306*, 872–876.
- (20) Kern, D.; Kern, G.; Neef, H.; Tittmann, K.; Killenberg-Jabs, M.; Wikner, C.; Schneider, G.; Hubner, G. *Science* **1997**, *275*, 67–70.
- (21) Reed, A. E.; Curtiss, L. A.; Weinhold, F. *Chem. Rev.* **1988**, *88*, 899–926.
- (22) Reed, A. E.; Weinhold, F.; Curtiss, L. A.; Pochatko, D. J. *J. Chem. Phys.* **1986**, *84*, 5687–5705.
- (23) Weinhold, F. Natural Bond Orbital Methods. In *The Encyclopedia of Computational Chemistry*; Schleyer, P. v. R., Ed.-in-Chief; John Wiley & Sons: Chichester, U.K., 1998.
- (24) Becke, A. D. *J. Chem. Phys.* **1993**, *98*, 5648–5652.
- (25) Lee, C.; Yang, W.; Parr, R. G. *Phys. Rev.* **1988**, *B37*, 785–789.
- (26) Frisch, M. J. et al. *Gaussian03*, revision C.02; Gaussian, Inc.: Wallingford, CT, 2004.
- (27) Dyda, F.; Furey, W.; Swaminathan, S.; Sax, M.; Farrenkopf, B.; Jordan, F. *Biochemistry* **1993**, *32*, 6165–6170.
- (28) Sax, M.; Pulsinelli, P.; Pletcher, J. *J. Am. Chem. Soc.* **1974**, *96*, 155–156.
- (29) Glendening, E. D.; Badenhoop, J. K.; Reed, A. E.; Carpenter, J. E.; Bohmann, J. A.; Morales, C. M.; Weinhold, F. *NBO 5.0 Program Manual. Natural Bond Orbital Analysis Programs*, NBO 5.0. Theoretical Chemistry Institute, University of Wisconsin: Madison, WI, 2001.

- (30) Bader, R. F. W.; Essén, H. *J. Chem. Phys.* **1984**, *80*, 1943–1960.
- (31) Jenkins, S.; Morrison, I. *Chem. Phys. Lett.* **2000**, *317*, 97–102.
- (32) Fradera, X.; Austen, M. A.; Bader, R. F. W. *J. Phys. Chem. A* **1999**, *103*, 304–314.
- (33) Biegler-Konig, F.; Schonbohm, J. *J. Comput. Chem.* **2002**, *23*, 1489–1494.
- (34) Sakaki, S.; Musashi, Y.; Ohkubo, K. *J. Am. Chem. Soc.* **1993**, *115*, 1515–1519.
- (35) Jordan, F.; Zhang, Z.; Sergienko, E. *Bioorg. Chem.* **2002**, *30*, 188–198.
- (36) Nemeria, N.; Baykal, A.; Joseph, E.; Zhang, S.; Yan, Y.; Furey, W.; Jordan, F. *Biochemistry* **2004**, *43*, 6565–6575.
- (37) Shin, W.; Oh, D. G.; Chae, C.-H.; Yoon, T.-S. *J. Am. Chem. Soc.* **1993**, *115*, 12238–12250.
- (38) Pletcher, J.; Sax, M.; Blank, G.; Wood, M. *J. Am. Chem. Soc.* **1977**, *99*, 1396–1403.
- (39) Arjunan, P.; Umland, T.; Dyda, F.; Swaminathan, S.; Furey, W.; Sax, M.; Farrenkopf, B.; Gao, Y.; Zhang, D.; Jordan, F. *J. Mol. Biol.* **1996**, *256*, 590–600.
- (40) Arduengo, A. J.; Goerlich, J. R.; Marshall, W. J. *Liebigs Ann. Recl.* **1997**, 365–374.
- (41) Wang, J.; Dong, H.; Li, S.; He, H. *J. Phys. Chem. B* **2005**, *109*, 18664–18672.
- (42) Fiedler, E.; Thorell, S.; Sandalova, T.; Golkik, R.; Konig, S.; Schneider, G. *Proc. Natl. Acad. Sci. U.S.A.* **2002**, *99*, 591–595.